Development of poly (ethylene-*co*-vinyl acetate) (EVA) nanocomposites and foams reinforced with reduced graphene oxide

http://dx.doi.org/10.1590/0370-44672023770067

Bruna Rossi Fenner[1,5]
https://orcid.org/0000-0002-6573-7383
Matheus Vinicius Gregory Zimmermann[2,6]
https://orcid.org/0000-0001-5851-7270
Lucas Repecka Alves[3,7]
http://orcid.org/0000-0001-5458-2403
Ademir José Zattera[4,8]
https://orcid.org/0000-0002-2198-4323
Ruth Marlene Campomanes Santana[1,9]
https://orcid.org/0000-0001-6843-9915

[1]Universidade Federal do Rio Grande do Sul - UFRGS, Programa de Pós-Graduação em Engenharia de Minas, Metalurgia e Materiais, Departamento de Materiais -DEMAT,
Porto Alegre – Rio Grande do Sul – Brasil.

[2]Universidade do Extremo Sul Catarinense - UNESC, Programa de Pós-Graduação em Ciências e Engenharia de Materiais,
Criciúma – Santa Catarina – Brasil.

[3]Universidade Federal de São Carlos - UFSCar, Programa de Pós-Graduação em Ciências dos Materiais, Sorocaba – São Paulo – Brasil.

[4]Universidade de Caxias do Sul - UCS, Programa de Pós-Graduação em Engenharia de Processos e Tecnologias, Caxias do Sul – Rio grande do Sul – Brasil.

E-mails: [5]bruna.fenner@hotmail.com, [6]matheus.vgz@gmail.com, [7]lucasrepecka@estudante.ufscar.br, [8]ademirjzattera@gmail.com, [9]ruth.santana@ufrgs.br

Abstract

Graphene and reduced graphene oxide are promising materials that are increasingly used in the field of polymer materials. In this study, reduced graphene oxide was prepared by chemical exfoliation of graphite, and subsequently, used in different amounts of 0.05, 0.2 and 2.0 wt.% in poly(ethylene-co-vinyl acetate) - EVA nanocomposites and foams. The approach used to prepare the reduced graphene oxide showed good efficiency with nanometer-scale particles and an average number of eight layers. Reduced graphene oxide in water suspension was introduced into the EVA by thermofusion using a closed mixer. Subsequently, sheets and foams were prepared by thermocompression molding using chemical expansion and crosslinking agents. The leading results suggest that the presence of reduced graphene oxide could change the cell morphology of the foam by increasing the cell density and decreasing its size. The sample containing 2 phr of reduced graphene oxide exhibited lower density and higher resistance to compression compared to pure EVA.

Keywords: EVA, foams, reduced graphene oxide, nanocomposites, thermofusion.

1. Introduction

Polymeric foams can be manufactured with a wide range of properties and for different applications. These materials represent one of the most important segments of the polymeric materials processing industry. Poly(ethylene-co-vinyl acetate) (EVA) foams, a copolymer with a low melting temperature (between 60 and 120 °C), are widely used in the footwear industry and EVA foams mats. The major properties associated with EVA foams are low-density relative to the original base polymer, good thermo-acoustic insulation properties, good wear resistance, and high impact strength. These properties are the consequence of the polymer's nature, void content (porosity), and cell morphology (Duan *et al*., 2014).

Over the last few years, several technologies have been used to produce polyolefin foams with further properties (Rodrigues-Perez *et al*., 2000; Rodrigues-Perez *et al*., 2012), and among the feasible modifications, the use of fillers and nanofillers stands out. The insertion of fillers in polymeric foams, in general, is carried out to reduce the product cost and/or increase the foam's rigidity. However, it might also be used to modify some specific properties, such as increasing the mechanical performance, thermal stability, cell nucleation (greater number of cells and smaller size per unit volume), and facilitate the pores opening around the cells, or give the material electrical properties, as in semiconductor polymers (Shan *et al*., 2012).

Different cell morphologies can be obtained depending on the type, size, and filler content used in polymeric foams (Zimmermann *et al*., 2014; Zimmermann *et al*., 2017), and recently, nano reinforced polymeric foams have gained attention, as significant morphological and mechanical variations are obtained using lower levels of nanofillers in the matrix polymeric, meaning less than 5%. Accordingly, when compared to the conventionally used reinforcing agents at the micrometric scale, the use of low levels of nanofillers might promote superior reinforcing and/or nucleating effects without compromising foam density (Ma *et al*., 2012).

Graphene has gained attention recently due to its fantastic properties. Graphene is a planar sheet of sp^2-bound carbon atoms densely packed in a honeycomb crystal lattice. It is considered the current thinnest material with remarkable properties, such as high thermal conductivity, mechanical strength, and excellent electronic properties. In addition to the aforementioned advantages, graphene materials own remarkable hydrophobic characteristics, obtained through modified graphene oxide, which has potential for further application in polymeric composites (Gadipelli & Guo, 2015; Fenner *et al*., 2018).

Graphene oxide (GO) is produced by the controlled graphite oxidation, and although it possesses polar chemical groups, such as hydroxyls, carbonyls, and epoxy groups. On the other hand, GO in its reduced form, the hydrophilic nature of the material reduces, due to the removal of a considerable part of the oxygen functional groups during the reduction (Liu *et al*., 2013). This monolayered carbon nanostructure is formed by carbons arranged in networks and has elevated mechanical, thermal, and electrical properties. But, due to the presence of small amounts of oxygen groups in reduced graphene oxide (GOr), it is still possible to disperse the fillers in water to homogeneously add the nanoparticles to the polymer matrix.

A study of mechanical properties of EVA foams with graphene for the applications in sport footwear developed by Lunchev *et al*. (2022). The authors report the development of EVA foams (with concentrations of 0.1 and 0.2 phr of graphene) presented higher flexural stiffness, lower compression force if squeezed by 50% and higher absorption of impact for foam with graphene compared to the referenced foam on real running shoes. Kuila *et al*. (2012) improved the mechanical and thermal properties of ethylene vinyl acetate copolymer with functionalized-graphene (with 1 wt.% loading), obtaining a material with higher tensile strength, storage modulus, thermal stability, and lower electrical resistivity comparing to pure EVA. Similar behavior was observed by Singh *et al*. (2020) in their study aimed to examine the mechanical behavior of graphene reinforced EVA composites at low strain rate loading under the influence of the varying composition of graphene (5 – 10 wt.%).

One of the greatest difficulties in the production of polymer nanocomposites, mainly using polyolefins, is based on the method of incorporating nanofillers into the polymer matrix. Drying the suspension with nanofillers usually promotes agglomeration of the fillers, and consequently, low dispersion in the polymer matrix. The incorporation of nanofillers by using the wet method (Zimmermann *et al*., 2017), uses the nanofillers suspension, without the pre-drying stage, which is considered a critical part on reinforced nanocomposites obtaining.

In the face of this, the objective of this study aims to synthesize reduced graphene oxide (GOr) by chemical exfoliation of graphite, and subsequently, produce EVA nanocomposites and foams with three different contents of GOr.

2. Experiment

2.1 Materials

Poly(ethylene-co-vinyl acetate) (EVA), type EVATENO 3019 PE, was supplied by Braskem SA, which has a vinyl acetate content of 19%, a specific mass of 0.940 $g.cm^{-3}$, a melt flow rate (MFR) (190 °C/2.16 Kg) of 2.5 $g.10\ min^{-1}$ and a melting point at 75 °C. The exothermic chemical expanding agent used was based on azodicarbonamide (ACA) supplied by Inbra Indústria Química Ltda. The zinc oxide (ZnO) was produced by Vetec and supplied by Sigma-Aldrich, which was used as an activator for the ACA decomposition. The crosslinking agent used was dicumyl peroxide (DCP), commercially known as Retilox DCP 99%.

To synthesize GOr, micronized graphite supplied by Sigma Aldrich was used as a precursor, which has

a molecular weight of 12.01 g.mol^{-1} and particles smaller than 20 µm. The necessary reagents for the synthesis were supplied by Didática company, namely: sulfuric acid (H_2SO_4, 98%), sodium nitrate ($NaNO_3$), potassium permanganate ($KMnO_4$), hydrogen peroxide (H_2O_2, 5%), barium chloride ($BaCl_2$), sodium borohydride ($NaBH_4$).

2.2 GOr production

The obtainment of GOr was carried out as Hummers & Offeman with adjustments, using a ratio of graphite, H_2SO_4 (mL) and $KMnO_4$ (g) of 1:22:3, similar to the original method and its multiple variations (~1:23:3) [10,14,15], although with reduced exfoliation and times. Based on this, the method of the present study consisted of adding 110 mL of H_2SO_4, previously cooled in a beaker with magnetic stirring in an ice bath, getting the acid to a temperature of ≤ 4 °C. Then, 5 g of graphite, 2.5 g of $NaNO_3$, and 15 g of $KMnO_4$ were slowly added. The initial temperature was kept and the experiment was performed under continuous magnetic stirring for 90 minutes. Afterward, the temperature was adjusted to 35 °C for 30 minutes, followed by the addition of 220 mL of deionized water, keeping the temperature below 80 °C (Liu *et al.*, 2013).

The permanganate anions (MnO_4^-) were eliminated by adding H_2O_2 until the color of the solution changed to greenish-yellow. After resting for 15 h, The solution underwent washing with deionized water following centrifugation (4500 rpm; 5 min) until the removal of H_2SO_4, as confirmed by the addition of a 1% weight $BaCl_2$ solution to the separated supernatant from the precipitate of graphene oxide. The presence of sulfate ions in the aqueous system was indicated by the formation of a white precipitate in the supernatant upon the addition of $BaCl_2$ (Cabrera *et al.*, 2016). The washed precipitate (pH 7) was placed in an oven at 50 °C for drying to obtain graphene oxide (GO). To reduce GO, 0.5 g of this material was added to 500 mL of deionized water and the mixture was sonicated (10 minutes; 50% measured at the maximum capacity of the 500W device) using a SONICS, model VC505 sonicator. A reflux system was then set up and the mixture was transferred to a round bottom flask containing 5 g of $NaBH_4$. The system was kept at 100 °C for 6 hours. Subsequently, the obtained GOr was filtered and dried in air (Li *et al.*, 2015).

2.3 EVA/GOr nanocomposites preparation and foaming

The production of EVA nanocomposites with GOr, in the form of plates, was carried out by thermofusion. 40 g of EVA were added in a closed mixing chamber (kneader lab Banbury mixer) at 120 °C and 100 rpm. Then, a GOr suspension was added dropwise during mixing. The total mixing time was 600 seconds. The studied filler contents were 0.05; 0.2; and 2.0 parts per hundred of resin (phr). The aqueous GOr suspension was sonicated (30 seconds; 50% amplitude) and added to the molten polymer matrix into the mixing chamber. The samples nomenclature was defined by its polymer matrix, followed by the filler content, and finished with the added filler, namely: EVA for the pure polymer; EVA-0.05/GOr for a composite with 0.05 phr of GOr; EVA-0.20/GOr for a composite with 0.20 phr of GOr; and EVA-2.00/GOr for a composite with 2.00 phr of GOr.

The incorporation of additives to produce EVA foams was carried out as described above, along with 1.2 g of azodicarbonamide, 0.2 g of zinc oxide and 0.8 g of dicumyl peroxide were added.

After the mixing time, the materials, still in molten state, were formed into plates using a thermos press, brand Shulz, which was used in a 5 x 80 x 80 mm mold and compressed for 120 seconds at 120 °C and 8 tons of closing cargo.

To expand the material, the preform (5 x 80 x 80 mm) was placed again in the mold for expansion at constant pressure, using a closing load of 8 tons at 140 °C for 10 minutes. Plate expansion takes place at the opening of the press.

2.4 Characterization

The X-ray photoelectron spectroscopy (XPS) was performed for the chemical characterization of the GOr, using an Omicron CHA (concentric hemispheric analyzer) model EA 125 equipment with an Al / Kα radiation source (1486.6 eV) and anode operated at 15 kV, 15 mA, 225 W. Powder samples were deposited on a copper strip in a molybdenum sample holder. Spectra were obtained with an energy pass of 50 eV and steps of 1 eV.

The X-ray diffractogram (XRD) was obtained using a Shimadzu brand equipment - model XRD-6000 (Japan), with monochromatic CuK α radiation of λ = 0.1542 nm, the voltage of 40 kV and current of 30 mA. The 2θ sweep was performed at an angular interval of 2 to 40°, with a 0.05° step and counting of 2 seconds per step (Lavoratti *et al.*, 2018). This technique was used to determine the number of GOr layers deposited by solvent evaporation on a slide with a reading area of 10 mm^2. The number of GOr layers was determined by Equations 1, 2, and 3.

$$d = \frac{n \times \lambda}{2 \times \text{sen}\theta} \quad (1)$$

$$L = \frac{k \times \lambda}{\beta \times \cos\theta} \quad (2)$$

$$N = \frac{L}{g + d} \quad (3)$$

Where d is the distance between the planes (nm), n is an integer, λ is the wavelength of the X-rays (0.1542 nm), θ is the Bragg angle (the half angle between the original beam), L is the apparent size of the crystallite (nm), K is the constant of proportionality (0.9), β is the broadening of the diffraction line measured at half the height of its maximum intensity (radian), N is the number of layers of the structure, and 'g' is the thickness of a graphene layer (0.1 nm). (Cullity & Stock, 2001; Osváth *et al*., 2007).

The GOr particle size was determined by dynamic light scattering (DLS) using a NANO-flex equipment with a DLS 180° system, which measures particle size distributions of suspensions and emulsions in the range of 0.3 nm to 10 µm and concentrations up to 40% by volume. For sample preparation, 0.5 % w/w load in 10 mL of grade water was added, subsequently, the suspension was sonicated for 30 seconds with 50% amplitude. The refractive index values were set to 1.33 and 2.38 for the dispersant (deionized water) and the material (carbon), respectively, according to a study carried out by Amaro-Gahete *et al*. (2019).

The mechanical-dynamic analysis (DMA) was performed on plate-shaped EVA composites with a TA Instruments device, DMA T800 model, using the flexion clamp. The double cantilever method was used with a 3 °C.min^{-1} heating rate, temperature range from -130 to 50°C, 1 Hz frequency, and 0.1% voltage amplitude (Zimmermann *et al*., 2014; Zimmermann *et al*., 2017; Neves *et al*., 2019).

Field emission scanning electron microscopy (MEV/FEG) and energy dispersion spectroscopy (EDS) were performed in a Tescan brand equipment used for morphological analysis, model FEG Mira 3, with a voltage of 15 kV. The EVA samples were previously coated with gold metal ions. For the foams, the observation area was analyzed in cross-section (horizontal direction) of the expanded sample, four points being selected in the sample to count the number of cells and their average diameter determination. The software used to measure the cell size was ImageJ. The cell population density per unit volume of the foamed composites (N_f) was determined from the SEM micrographs using Equations 4 and 5.

$$V_f = 1 - \frac{\rho_f}{\rho_p} \quad (4)$$

$$N_f = \left(\frac{nM^2}{A}\right)^{3/2} \cdot \left(\frac{1}{1 - V_f}\right) \quad (5)$$

Where: V_f is the void content; ρ_f is the density of the expanded composite (g.cm^{-3}); ρ_p is the density of the polymer or composite (g.cm^{-3}); N_f is the cell density (number of cells per cm³); n is the number of cells in the micrograph; A is the micrograph area (cm²); and M is the magnification of the micrograph.

The thermal properties of EVA nanocomposites, before expansion, were evaluated using differential scanning calorimetry (DSC) in a SHIMADZU model DSC-60 instrument, in the temperature range of 23 to 200 °C, a rate of 10 °C.min^{-1} and controlled atmosphere of nitrogen (50 mL.min^{-1}). The crystallinity index was calculated using Equation 6:

$$X_c = \frac{\Delta H_m}{\Delta H_0 \, x \, w} \, x \, 100 \quad (6)$$

Where X_c is the crystallinity index (%), ΔH_m is the fusion enthalpy of the sample (Jg^{-1}), ΔH_0 is the fusion enthalpy for 100% crystalline polyethylene (293 Jg^{-1}) and w is X_c correction for the polymer content in the composition.

The foams apparent density was calculated by the sample mass (g) and volume (cm³) ration. Five replicate measurements, at different locations in the expanded plate, were made for each sample.

The compressive strength analysis was performed using a TA Instruments, model DMA T800, with compression clamp. Samples with dimensions of 5 x 5 x 5 mm were used. The applied force ramp was from 3 N.min^{-1} to 18 N (equipment limit). The tension necessary to reduce the thickness of the specimen by 10, 30, 50 and 70% of its initial thickness was evaluated.

3. Results and discussion

3.1 Characterization of GOr

GOr was characterized by morphological analysis (MEV-FEG), analysis of chemical composition and O:C ratio (EDS and XPS), quantification of the number of layers (XRD) and analysis of particle size and its distribution and frequency in solution (DLS). Figure 1 shows the microscopic images and energy dispersion spectrum of GOr. Analyzing the micrograph in Figure 1a, it can be seen that the GOr has exfoliated structures that have the appearance of "crumpled paper sheets", and numerous sheet edges can also be seen (lighter regions within the outlines of darker regions). In Figure 1b, at higher magnification, the presence of loose leaves with high transparency can be seen, indicating that these structures have few layers. Using the EDS spectrum shown in Figure 1c, it was possible to perform a qualitative analysis of the GOr composition, with some preliminary considerations.

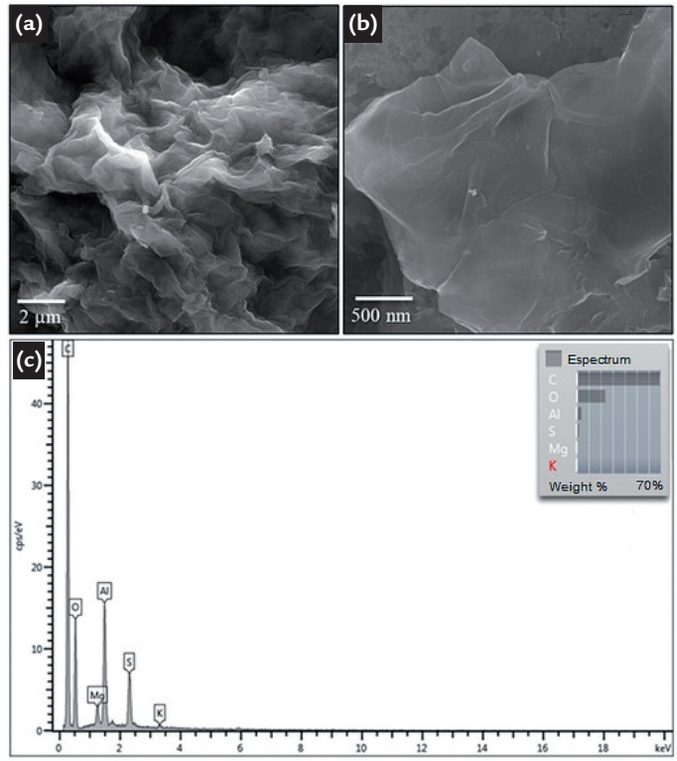

Figure 1 - (a) and (b) Micrographs obtained by MEV-FEG and (c) EDS spectrum of GOr.

First, the stub used for GOr deposition is mainly aluminum (Al) and also contains magnesium (Mg) and silicon (Si). Therefore, these elements have been disregarded in the discussion in this work. In addition, elements below 1% are classified as trace elements, and since this is a low precision area, potassium (K) has also been disregarded. GOr is thus essentially Carbon and Oxygen, with a small amount of Sulphur. The presence of S and even traces of K can be explained by the fact that GOr was obtained by a method using sulphuric acid (H_2SO_4) and potassium permanganate ($KMnO_4$), as well as by the original method of Hummers & Offeman and its studied variants (Hummers & Offeman, 1958; Gao *et al*., 2009; Yu *et al*., 2016).

In addition to the qualitative analysis, a semi-quantitative analysis was performed using the spectrum in mass percent of C, O and S. This analysis did not include the trace elements and stub alloy elements identified in the spectra. Thus, the GOr gave values of 73.5% C, 25.4% O and 1.1% S. Guerrero-Contreras and Caballero-Briones (2015) studied the method of Hummers & Offeman for GOr producing, and obtained an average percentage of 77.7% C and 20.7% O, and in the present study, they presented similar percentages.

Figure 2 shows the XPS spectrum and the GOr diffractogram, in which a peak in the C1s signal of around 287 eV and a peak in the O1s signal of around 534 eV can be observed. Similar results were reported by Marchon *et al*. (1988). The graphite sample studied by Jeon *et al*. (2013) showed a sharp peak in the C1s signal and a more subtle one in the O1s signal. In the GOr sample, peaks are observed in the same signals, but with a stronger O1s signal compared to graphite, leading to an equilibrium in the ratio of C1s and O1s peaks. Based on the ratio between the areas of C1s and O1s peaks, the C/O ratio was calculated, which gives a ratio of 1.5:1 for the Gor sample, which means it presents an average of 1.5 C molecules for every O molecule. In the study by Fu *et al*. (2013), the C/O ratio was calculated from the XPS spectra, as well presenting 2.7:1 for graphene oxide, indicating that more oxygen was retained compared to the GOr sample in the present study.

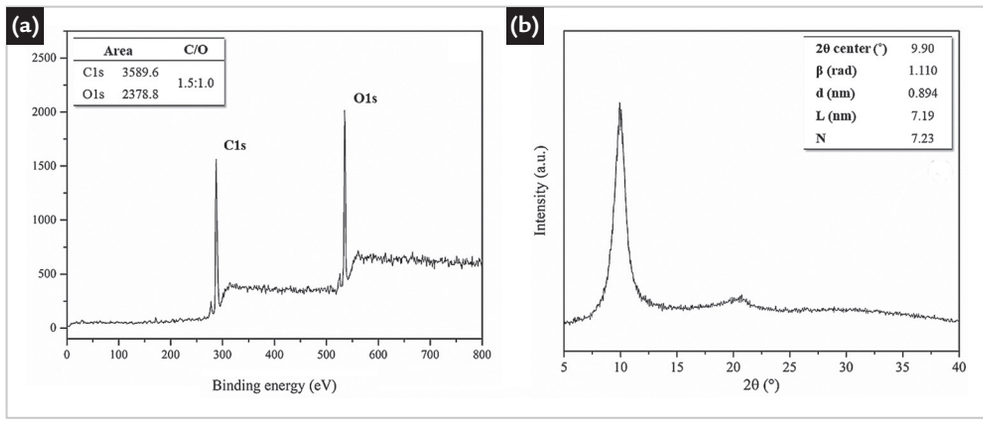

Figure 2 - (a) XPS spectrum and (b) GOr diffractogram.

Figure 2b shows the diffractogram of the GOr sample obtained by XRD and the data extracted from it used to calculate the number of layers, as well as the calculated data, including the number of layers in the sample. A prominent diffraction peak at 2θ = 9.9° was identified in the diffractogram, which corresponds to the (001) plane characteristic of graphene oxides according to Gharib *et al.* (2015) and King *et al.* (2016). This is due to the intercalation of functional groups between the graphite layers, which leads to an increase in the interplanar distance (Kashyap *et al.*, 2014). A relatively weak and broad shoulder was observed around 2θ = 21°, related to a reduction stage according to the study of Huang *et al.* (2018) about the hydrothermally reduction process of graphene oxide, which indicates the coexistence of reduced graphene oxide and graphene oxide. From the analysis of plane (002), it can be observed that there is no peak around 27.2° which is the characteristic graphite peak as presented in the study by Perera *et al.* (2018). Since a graphite precursor was used to obtain GOr, this indicates that graphite is no longer present in the material obtained.

According to the results presented in the table in Figure 2b, the values of 'L' (crystallite size) and 'd' (interplanar spacing) were 0.894 and 7.19 nm, respectively, resulting in a value of N (number of layers) of approximately 8 layers. According to the ISO/TS 80004-13:2017 standard, GOr should be classified as reduced graphene oxide, defined as the reduced oxygen content form of graphene oxide. The standard specifies that the reduction process can be achieved through various methods, including chemical, thermal, microwave, photo-chemical, photo-thermal, or microbial/bacterial approaches, or by exfoliating reduced graphite oxide. It is important to note that, in practical terms, full reduction to graphene may not occur, and some oxygen-containing functional groups may persist, preventing all sp3 bonds from reverting to an sp2 configuration. Additionally, different reducing agents can result in varying carbon-to-oxygen ratios and chemical compositions in reduced graphene oxide. The morphological variations of reduced graphene oxide, as outlined in the standard, include platelets and worm-like structures. Therefore, in accordance with the ISO/TS 80004-13:2017 standard, GOr should be accurately characterized as reduced graphene oxide rather than graphene with few layers.

The GO, a single-layer material, is characterized by a high oxygen content, typically denoted by C/O atomic ratios of approximately 2.0, with variations depending on the synthesis method. The ISO/TS 80004-13:2017 standard defines reduced graphene oxide, not solely based on the number of layers but also considering the oxygen content, specifically the C/O atomic ratios. As GOr is identified as the "reduced oxygen content form of graphene oxide," and graphene oxide is known for having C/O atomic ratios of around 2.0. It follows that GOr's classification extends beyond its layer count. GOr is categorized not only by its number of layers but also by possessing a C/O atomic ratio < 2.0, in accordance with the standard.

Perera *et al.* (2018) studied the impact of oxygen on the structure and exfoliation of graphene oxide in relation to the oxidation time, where they found values for 'd' between 0.892 and 0.925 nm and values for 'L' in the range of 16.9 – 18.3 nm, with 19 to 20 layers of the material. Comparing these values with the GOr's, it can be verified that the interplanar distance was similar, but the size of the crystallite in the study in comparison was doubled, which justifies their high number of layers.

Figure 3 shows the DLS results of GOr sample, where "d" axis represents the particle size, 'Qr' is the distribution curve and 'q*r' is the frequency that the particles of a certain size appear. In addition, the data generated in the same report on the representative volumes and the diameter and width of each volume are presented.

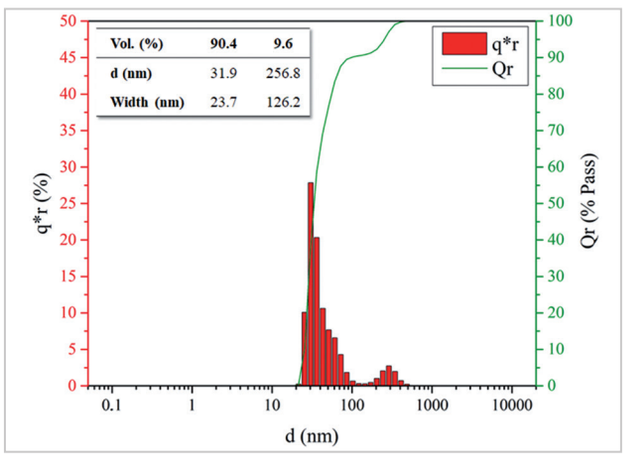

Figure 3 - DLS particle size distribution of GOr.

On this basis, it can be concluded that the particle size is well captured with an average value of 31.9 nm in diameter and 23.7 nm in width, corresponding to 90.4% of the analyzed sample volume. Mean values of 256.8 nm in diameter and 126.2 nm in width were found for the rest of the analyzed sample volume (9.6%). Frankberg *et al.* (2015) also obtained graphene oxide using the method of Hummers & Offeman but obtained a particle size distribution in which the largest volume had a size close to 1000 nm and the smallest volume had a size close to 100 nm, in contrast to the behavior of the present study. Kashyap *et al.* (2014) studied the particle size distribution of graphene oxide at different pH values using DLS, where the normal particle size was 600 nm with a maximum of 1000 nm.

3.2 Characterization of nanocomposites and EVA foams reinforced with GOr

Figure 4 shows the dynamic mechanical analysis of EVA and its composites (unexpanded). In Figure 4a, it can be seen from the storage modulus that the composites show a larger mechanical response in the glassy region below -25°C compared to pure EVA, and the higher the GOr content, the higher the value of the storage modulus. This difference in modulus response decreases above -25°C. The presence of GOr can affect the molecular mobility of EVA in different ways. The strong interaction between the filler and the matrix reduces the molecular mobility of the polymer, which is more noticeable in the glassy region. Monteserín *et al.* (2017) mentions that the increase in the amount of GOr can induce a greater crosslinking density between the polymer chains. Thus, the addition of GOr on the polymer indicates an effective crosslinking network, which explains the increase in the value of the storage modulus.

From the loss modulus shown in Figure 4b, an event related to the glass transition of the material at about -25°C was identified and no significant variations were found in the transition temperature of the analyzed materials at different charge contents. From the Tan-Delta diagram in Figure 4c, it can be seen that EVA has two distinct relaxation events, the first being near -10°C and the second near 25°C. According to Sefadi & Luyt (2012), the first relaxation at -25°C is due to the movement of chain segments with three or four methylene groups (-CH_2-) and is related to the glass transition of the material (T_g). Below the T_g, the molecular chain segments are frozen and the damping is low, so that little energy is stored in the elastic deformations. In the rubbery region, the damping is higher than in the glassy state because the molecular segments are free to move, resulting in lower stiffness, and excess energy is dissipated in the form of heat. The second relaxation at 25°C may be related to the movement of the amorphous regions within the crystalline phase, i.e., to the realignment of the defect regions between the crystals, or it may be considered as an expression of the relaxation of the flexible chains of vinyl acetate groups present in EVA copolymer chains (Sefadi & Luyt, 2012).

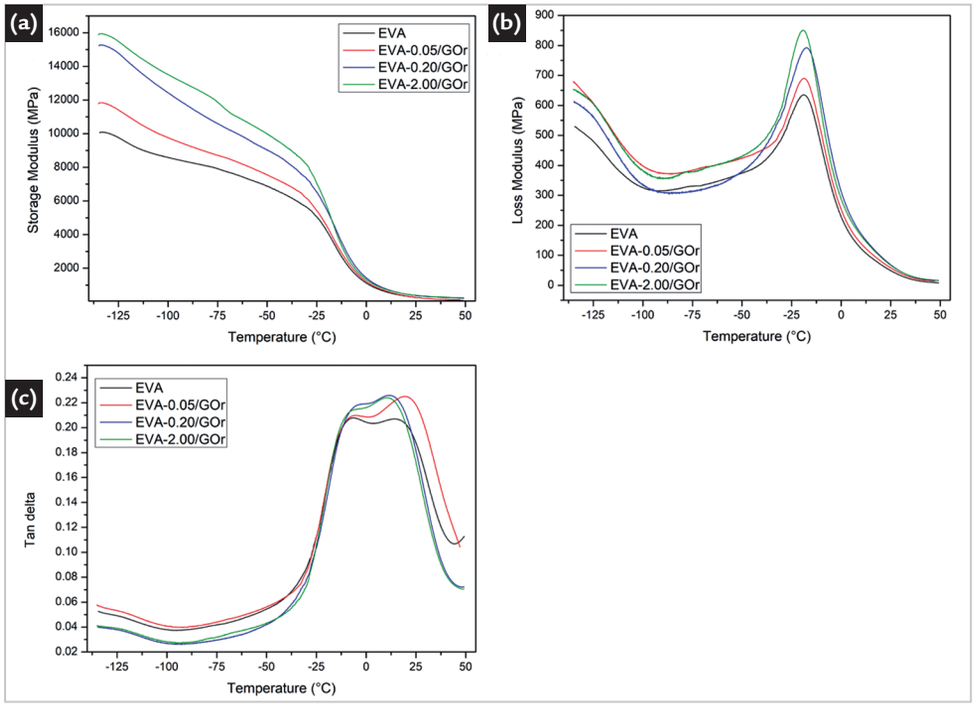

Figure 4 - Dynamic mechanical analysis of EVA and composites, being: (a) storage module; (b) loss modulus and (c) tan delta.

Table 1 shows the thermal properties of EVA nanocomposites (unexpanded) obtained by DSC. It is observed that the presence of GOr tends to increase the crystallinity of EVA, a result reported by Tham *et al.* (2016). The presence of fillers tends to promote heterogeneous nucleation, where the presence of nuclei favors the formation of crystals. Compared to pure EVA, a slight decrease in the melting temperature and an increase in the crystallization temperature upon cooling are observed for both events (1st and 2nd heating). The non-linear relationship observed in the increase of GOr content and crystallinity percentage can be attributed to the complex interactions between GOr and the polymer matrix, including factors, such as agglomeration, since graphene has a tendency to agglomerate in the polymer matrix, disruption of polymer chain ordering, interactions with functional groups, and influence on nucleation and growth processes (Yuan *et al.*, 2012).

For the preparation of polymer foams, Xu *et al.* (2007) point out that it is more difficult to control the cellular structure of a semi-crystalline polymer foam compared to a fully amorphous polymer (Tham *et al.*, 2016). The gases do not dissolve in crystalline regions and the dispersion of the gas formed during the process is usually not uniform. However, this phenomenon is more pronounced in foams produced with physical expanders. Foams produced with chemical expanders are generally produced at high temperatures where the crystal structure has little influence (Xu *et al.*, 2007; Nofar & Park, 2014). Considering the processing and expansion method used in this experiment, even if the foaming temperature is above the melting temperature of EVA, at which theoretically only the amorphous phase would exist, the onset of decomposition of the expanding agent, as well as nucleation of small cells, could occur at lower temperatures, which would affect

cell morphology. However, it should also be noted that the presence of fillers has a greater impact on the formation of cell morphology. Nofar & Park (2014) mention that the crystallinity of the polymer during foaming can have a significant impact on cell nucleation, as cells can form at the boundary of additives (e.g. fillers), as well as at the boundary of crystals.

Table 1 - Thermal properties of EVA and non-expanded nanocomposites obtained by DSC.

Sample	First heating			Cooling	Second heating		
	T_m	ΔH_m	X_c	T_c	T_m	ΔH_m	X_c
	°C	$J.g^{-1}$	%	°C	°C	$J.g^{-1}$	%
EVA	91.4	24.4	8.3	64.9	90.2	10.7	3.6
EVA-0.05/GOr	87.6	35.4	12.1	67.7	88.3	24.8	8.5
EVA-0.20/GOr	86.8	34.5	11.8	68.2	87.6	18.3	6.2
EVA-2.00/GOr	86.9	36.5	12.7	68.6	87.3	20.9	7.3

Table 2 shows the physical properties in terms of density of the EVA samples, before and after expansion. It is possible to note that, with the exception of the sample EVA -2.00/GOr, expanded compounds presented similar values, which with the addition of the filler did not present a significant variation in density considering the error. However, the same behavior was not observed for the composites before expansion, which showed a slight tendency towards increasing density with increasing filler content. The foam sample with the lowest density among all those prepared was EVA -2.00/GOr, which has the highest filler content. The density of foams depends on the morphological structure of the cells, such as the size, the regularity of the size and the number of cells per unit area. Similar results were presented by Lunchev *et al.* (2022) for EVA foams filled with different contents of graphene, reaching 140 ± 20 $Kg.m^{-3}$ for EVA foam with 0.2 phr of GOr.

Table 2 - Physical properties of nanocomposites and EVA foams with different GOr contents.

Sample	Apparently density ($Kg.m^{-3}$)		V_f (%)
	Unfoamed	Foam	
EVA	891.75 ± 45.44	134.96 ± 11.70	86.27
EVA-0.05/GOr	894.23 ± 34.69	135.70 ± 11.57	82.14
EVA-0.20/GOr	901.80 ± 49.35	138.42 ± 9.33	83.06
EVA-2.00/GOr	907.77 ± 30.48	86.26 ± 8.53	89.16

The photographs of EVA foams without filler and with the different contents of GOr studied are presented in Figure 5(a), where it is possible to observe the characteristic gray color of the added filler as well as its intensification as the GOr content is increased. In Figure 5 (b) and (c), micrographs of the expanded EVA and EVA-2.00/GOr samples at the same scale are presented, respectively. In these images, it is not possible to verify differences on the surface of the foams. However, in Figure 5(d), it was possible to identify the presence of GOr on the EVA-2.00/GOr surface despite the low filler content added to the foam.

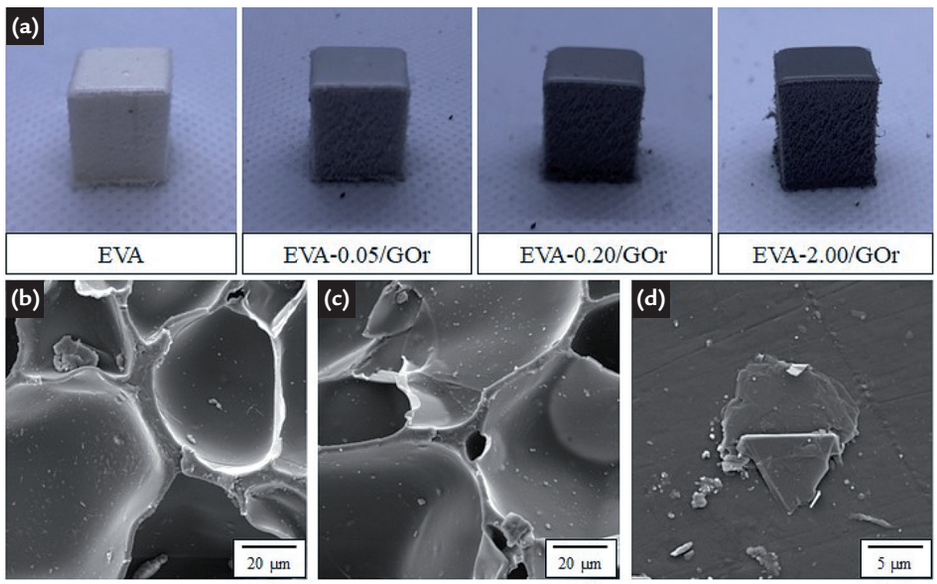

Figure 5 - Photographs of EVA foams samples (a), and micrographs obtained by SEM, being: (b) EVA; (c) and (d) EVA-2.00/GOr.

Figure 6 shows the morphological analysis of the EVA foams with different GOr contents. It can be seen that all foams have a morphological structure consisting mainly of closed cells. For the samples EVA-0.20/GOr and EVA-2.00/GOr, a decrease in cell size and an increase in cell density can be observed compared to pure EVA.

Depending on the type, size and concentration of the charge used in the composition of polymer foams, different morphologies and cell densities can be obtained (Doroudiani & Kortschot, 2004; Zimmermann *et al*., 2014; Zimmermann *et al*., 2017). The cell density is affected by both the content and size/diameter of the filler. In general, the presence of the filler acts as a heterogeneous nucleation point for the cells, considering that the presence of micropores or voids at the polymer-charge interface allows the migration of the generated gas into these regions, thus promoting the spread and growth of the cell from this location (Trone, 1996). The presence of two groups of cells (two different sizes) is discussed by Duan *et al*. (2014) and defined as bimodal foam. In the development of a polyolefin foam, the decomposition of the blowing agent must first promote the formation of several small cells within the polymer matrix, and during the growth of these cells, coalescence cannot occur until the polymer matrix cures (cross-linking).

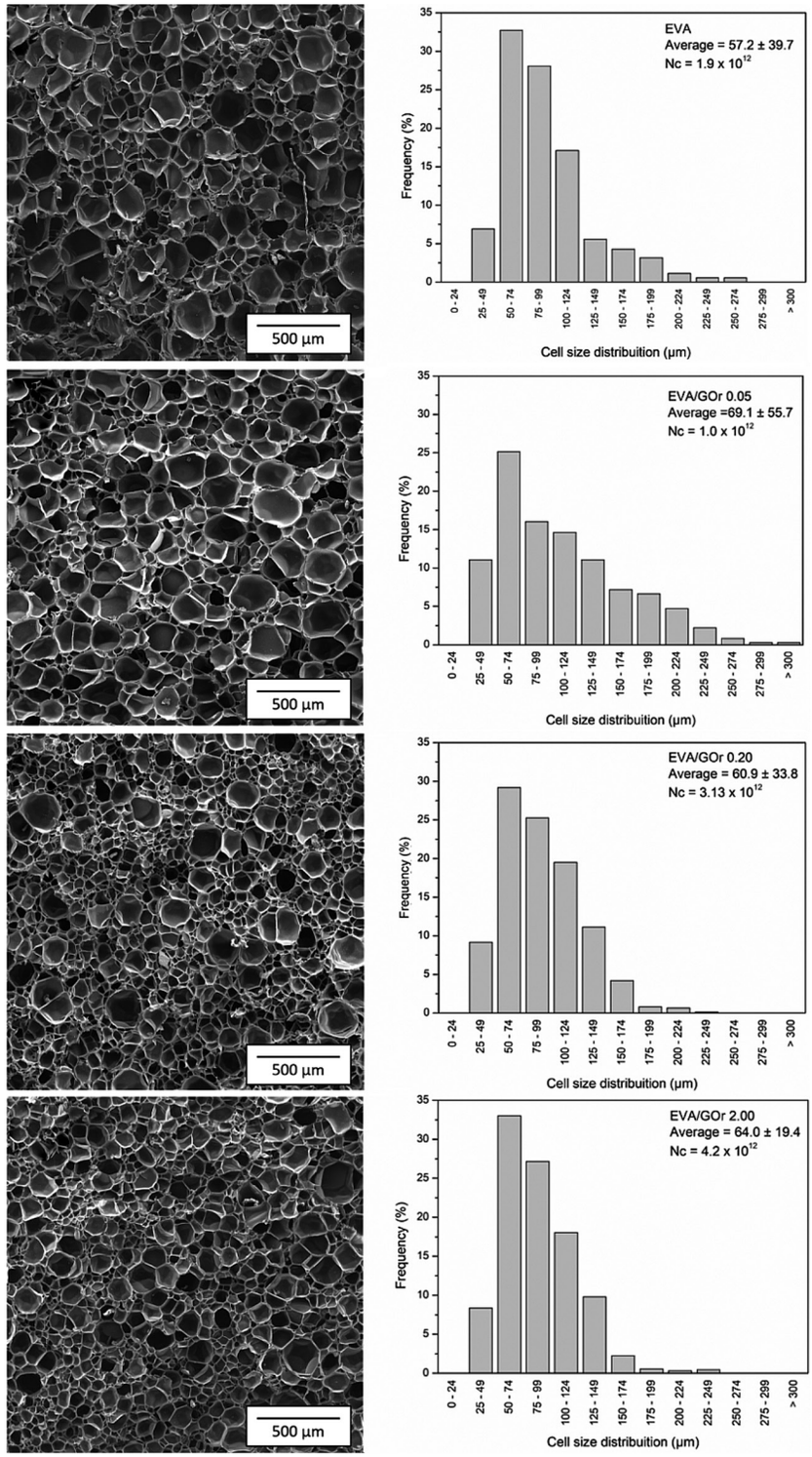

Figure 6 - Micrograph obtained by SEM and analysis of the cell size distribution of EVA foams with different levels of GOr.

As mentioned earlier, the filler acts as nucleating agent for cell formation. However, if during the incorporation of the filler into the polymer matrix, these fillers agglomerate and aggregate, this phenomenon can promote cell coalescence and the formation of larger cells. Thus, the formation of a morphology with bimodal cells may be associated with the filler agglomeration, where small nanometer-scale particles and agglomerated micrometer-scale particles may coexist in the polymer. Another factor to consider is the chemical affinity of the particles with the polymer matrix. A good interface (contact area between the dispersed phase and the polymer matrix) favors the formation of larger cells, since the gas from the blowing agent tends to migrate to the area of lower resistance and continue its growth from this point (Duan *et al.*, 2014).

Figure 7 shows the stress-strain curves in an analysis of the compressive strength of EVA foams with different GOr contents. The edges of the foam cells in the region of elastic deformation, up to 10% deformation, experience elastic bending from which they fully recover when the load is removed without the cell cracking or deforming. In the plateau region, between 10 and 50% deformation, the foam deforms significantly without increasing the stress. This is because the edges and solid contours of the cells begin to collapse plastically; the cells deform and disappear while the individual elements and foam rapidly thicken. In the area of compression, the stress increases rapidly without a large increase in deformation, because since a large part of the cells have already collapsed and deformed, the base polymer material itself begins to be compressed, leading to a rapid increase in the resistance of the foam, above 50% deformation (Zimmermann *et al.,* 2017; Fenner *et al.*, 2018; Eaves, 2004).

According to Lunchev *et al.* (2022), the optimal property of a foam sample is low density and high compressive stress for applications in high performance footwear. Considering that EVA-2.00/GOr foams had lower density, as shown in Table 2, and greater compression resistance at 50% deformation, the optimal formula for application in the footwear industry would be with 2 phr of GOr. Comparing to the foams produced by Lunchev *et al.* (2022), the EVA-0.20/GOr (0.25 MPa) presented a higher compressive strength than the EVA foam with 0.20 phr of GOr (0.13 MPa), approximately the doble of it. It can be related with the compatibility of the filler with the polymer matrix.

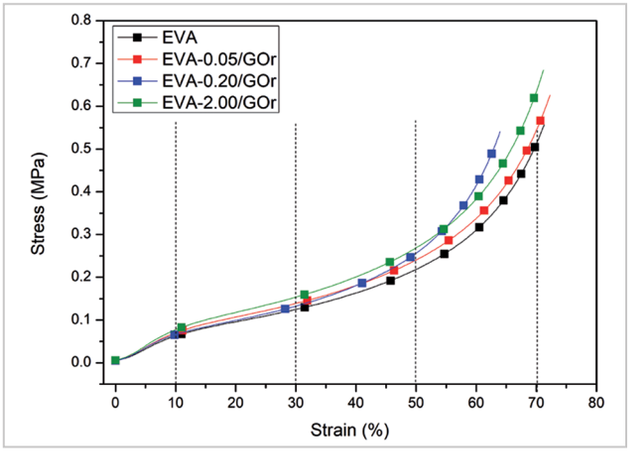

Figure 7 - Stress × strain curve of an analysis of compressive strength of EVA foams with different GOr contents.

It can be concluded that the presence of GOr, compared to pure EVA, increases the mechanical strength of the foam at all stages of deformation. Reduced cell size and increased cell density tend to result in stiffer foams. The connection between foam density and mechanical properties is also important. The samples EVA-0.05/GOr and EVA-0.20/GOr had higher density than the pure EVA and stiffer behavior than the pure EVA, but the sample EVA-2.00/GOr had the lowest density of all the samples studied and better mechanical behavior. The increase in the frequency of small cells with increasing filler content shown in Fig. 6, corroborates the increase in foam stiffness, as well as the increase in foam density.

4. Conclusion

Based on the characterization of GOr, it is possible to confirm the exfoliation of graphene layers present in the crystalline structure of graphite, which can be observed by microscopic images for the presence of loose sheets as well as nanoscale structures. The method of incorporation of GOr in EVA showed good dispersion and homogeneous distribution. The presence of GOr alters the crystallinity of the polymer and molecular mobility at low temperatures. In foam production, the presence of GOr alters the cell morphology, increasing the cell density of the foams, and consequently, a higher compressive strength was also observed in the GOr reinforced samples. Among the analyzed compositions, the sample EVA-2.00/GOr showed the best relationship between the mechanical properties and the low density.

Acknowledgements

The authors would like to thank Coordination for the Improvement of Higher Education Personnel (CAPES) and National Council for Scientific and Technological Development (CNPq) for the financial support.

References

AMARO-GAHETE, J.; BENÍTEZ, A.; OTERO, R.; ESQUIVEL, D.; JIMÉNEZ-SANCHIDRIÁN, C.; MORALES, J.; CABALLERO, A.; ROMERO-SALGUERO, F. J. A comparative study of particle size distribution of graphene nanosheets synthesized by an ultrasound-assisted method. ***Nanomaterials,*** v. 9, n. 152, p. 1-16, 2019.

CABRERA, L. C.; BAUMGARTEN, M. G. Z.; NIENCHESKI, L. F. H.; SPENGLER, A. Adaptação do método turbidimétrico para a análise de sulfato em amostras de águas estuarinas e marinhas. ***Vetor,*** 16, p. 7-10, 2016.

CULLITY, B. D.; STOCK, S. R. ***Elements of X-Ray diffraction***. 3. ed. Nova Jersey, Upper Saddle River: Prentice Hall, 2001.

DOROUDIANI, S.; KORTSCHOT, M. T. Expanded wood fiber polystyrene composites: processing – structure – mechanical properties relationships. ***J Thermoplast Compos Mater,*** 17, p. 13-30, 2004.

DUAN, Z.; MA, J.; XUE, C.; DENG, F. Effect of stearic acid/organic montmorillonite on EVA/SA/OMMT nanocomposite foams by melting blending. ***J Cell Plast,*** v. 50, n. 3, p. 263-277, 2014.

EAVES, D. ***Handbook of polymer foams.*** Rapra Technology, UK, 2004. Cap. 1, p. 1-8.

FENNER, B. R.; ZIMMERMANN, M. V. G.; DA SILVA, M. P.; ZATTERA, A. J. Comparative analysis among coating methods of flexible polyurethane foams with graphene oxide. ***J Mol Liq,*** 271, p. 74-79, 2018.

FRANKBERG, E. J.; GEORGE, L.; EFIMOV, A.; HONKANEN, M.; PESSI, J.; LEVANEN, E. Measuring synthesis yield in graphene oxide synthesis by modified hummers method. ***Fullerenes Nanotubes Carbon Nanostruct,*** 23, p. 755-759, 2015.

FU, C.; ZHAO, G.; ZHANG, H.; LI, S. Evaluation and characterization of reduced graphene oxide nanosheets as anode materials for lithium-ion batteries. ***Int J Electrochem Sci,*** v. 8, n. 5, p. 6269-6280, 2013.

GADIPELLI, S.; GUO, Z. X. Graphene-based materials: synthesis and gas sorption, storage and separation. ***Prog Mater Sci,*** 69, p. 1-60, 2015.

GAO, W.; ALEMANY, L. B.; CI, L.; AJAYAN, P. M. New insights into the structure and reduction of graphite oxide. ***Nat Chem,*** 1, p. 403-408, 2009.

GHARIB, A.; FARD, L. V.; PESYAN, N. N.; ROSHANI, M. A new application of nano- graphene oxide (NGO) as a heterogeneous catalyst in oxidation of alcohols types. ***Chem J,*** v. 1, n. 4, p. 151-158, 2015.

GUERRERO-CONTERAS, J.; CABALLERO-BRIONES, F. Graphene oxide powders with different oxidation degree, prepared by synthesis variations of the Hummers method. ***Mater Chem Phys,*** 153, p. 209-220, 2015.

HUANG, H.; SILVA, K. K. H.; KUMARA, G. R. A.; YOSHIMURA, M. Structural evolution of hydrothermally derived reduced graphene oxide. ***Sci Rep,*** v. 8, n. 6849, p. 1-9, 2018.

HUMMERS, W. S.; OFFEMAN, R. E. Preparation of graphitic oxide. ***J Am Chem Soc,*** 80, p. 1339, 1958.

INTERNATIONAL ORGANIZATION FOR STANDARDIZATION. ***ISO/TS 80004-13:2017*** - part 13: graphene and related two-dimensional (2D) materials.

JEON, I.; CHOI, H.; JU, M. J.; CHOI, I. T.; LIM, K.; KO, J.; KIM, H. K.; KIM, J. C.; LEE, J.; SHIN, D.; JUNG, S.; SEO, J.; KIM, M.; PARK, N.; DAI, L.; BAEK, J. Direct nitrogen fixation at the edges of graphene nanoplatelets as efficient electrocatalysts for energy conversion. ***Sci Rep,*** v. 3, n. 2260, 2013.

KASHYAP, S.; MISHRA, S.; BEHERA, S. K. Aqueous colloidal stability of graphene oxide and chemically converted graphene. ***J Nanopart,*** p. 1-6, 2014.

KING, A. A. K.; DAVIES, B. R.; NOORBEHESHT, N.; NEWMAN, P.; CHURCH, T. L.; HARRIS, A. T.; RAZAL, J. M.; MINETT, A. I. A new raman metric for the characterisation of graphene oxide and its derivatives. ***Sci Rep,*** 6, p. 1-6, 2016.

KUILA, T.; KHANRA, P. MISHRA, A. K.; KIM, N. H.; LEE, J. H. Functionalized-graphene/ethylene vinyl acetate co-polymer composites for improved mechanical and thermal properties. ***Polym Test,*** 31, p. 282-289, 2012.

LAVORATTI, A.; ZATTERA, A. J.; AMICO, S. C. Mechanical and dynamic-mechanical properties of silane-treated graphite nanoplatelet/epoxy composites. ***J Appl Polym Sci,*** 46724, p. 1-10, 2018.

LI, B.; LIU, X.; ZHANG, X.; CHAI, W.; MA, Y.; TAO, J. Facile preparation of graphene-coated polyurethane sponge with superhydrophobic/superoleophilic properties. ***J Polym Res,*** v. 22, n. 10, p. 1-6, 2015.

LIU, Y.; MA, J. K. WU, T. WANG, X. G.; HUANG, G. R.; LIU, Y.; QIU, H. X.; LI, Y.; WANG, Y.; GAO, J. P. Cost-effective reduced graphene oxide-coated polyurethane sponge as a highly efficient and reusable oil-absorbent. ***ACS Appl Mater Interfaces,*** 5, p. 10018-10026, 2013.

LUNCHEV, A. V.; KASHCHEEV, A.; TOK, A. L. Y.; LIPIK, V. Mechanical characteristics of poly (ethylene vinyl acetate) foams with graphene for the applications in sport footwear. ***Polym Test,*** 113, p. 107688, 2022.

MA, J.; DUAN, Z.; XUE, C.; DENG, F. Morphology and mechanical properties of EVA/OMMT nanocomposite foams. ***J Thermoplast Compos Mater,*** v. 26, n. 4, p. 555–569, 2012.

MARCHON, B.; CARRAZZA, J.; HEINEMANN, H.; SOMORJAI, A. TPD and XPS studies of oxygen, carbon dioxide, and water adsorption on clean polycrystalline graphite. ***Carbon,*** v. 26, n. 4, p. 507-514, 1988.

MONTESERÍN, C.; BLANCO, M.; ARANZABE, E.; ARANZABE, A.; LAZA, J. M.; LARRAÑAGA-VARGA, A.; VILAS, J. L. Effects of graphene oxide and chemically-reduced graphene oxide on the dynamic mechanical properties of epoxy amine composites. ***Polymers,*** v. 9, n. 9, 449, 2017.

NEVES, R. M.; LOPES, K. S.; ZIMMERMANN, M. V. G.; POLETTO, M.; ZATTERA, A. J. Characterization of polystyrene nanocomposites and expanded nanocomposites reinforced with cellulose nanofibers and nanocrystals. ***Cellulose,*** 26, p. 4417-4429, 2019.

NOFAR, M.; PARK, C. B. Poly (lactic acid) foaming. ***Prog Polym Sci,*** 39, p. 1721-1741, 2014.

OSVÁTH, Z.; DARABONT, A.; NEMES-INCZE, P.; HORVÁTH, E.; HORVÁTH, Z. E.; BIRÓ, L. P. Graphene layers from thermal oxidation of exfoliated graphite plates. ***Carbon,*** v. 45, n. 15, p. 3022-3026, 2007.

PERERA, D.; ABEYWICKRAMA, A.; ZEN, F.; COLAVITA, P. E.; JAYASUNDARA, D. R. Evolution of oxygen functionalities in graphene oxide and its impact on structure and exfoliation: an oxidation time based study. ***Mater Chem Phys,*** 220, p. 417-425, 2018.

RODRIGUES-PEREZ, M. A.; SIMOES, R. D.; ROMAN-LORZA, S.; ALAVAREZ-LAINEZ, M.; MONTOYA--MESA, C.; CONSTANTINO, C. J. L.; DE SAJA, S. A. Foaming of EVA/starch blends: characterization of the structure, physical properties, and biodegradability. ***Polym Eng Sci,*** 52, p. 62-70, 2012.

RODRIGUES-PEREZ, M. A.; VELASCO, J. I.; ARENCÓN, D.; ALMANZA, O.; DE SAJA, S. A. Mechanical characterization of closed-cell polyolefin foams. ***J Appl Polym Sci,*** 75, p. 156-166, 2000.

SEFADI, J. S.; LUYT, A. S. Morphology and properties of EVA/empty fruit bunch composites. ***J Thermoplast Compos Mater,*** v. 25, n. 7, p. 895-914, 2012.

SHAN, C. W.; IDRIS, M. I. GHAZALI, M. I. Study of flexible polyurethane foams reinforced with coir fibres and tyre particles. ***Int J Appl Phys Math,*** 2, p. 123-130, 2012.

SINGH, A. K.; KUMAR, D.; JINDAL, P. Influence of graphene on mechanical behavior of EVA composite at low strain rate loading. *In*: PRAKASH, C.; SINGH, S.; KROLCZYK, G.; PABLA, B. (ed.) ***Advances in materials science and engineering.*** Singapore: Springer,2020. (Lecture Notes in Mechanical Engineering).

THAM, D. Q.; TRANG, N. T. T.; CHINH, N. T.; GIANG, N. V.; LAM, T. D.; HOANG, T. Sustainable composite materials based on ethylene-vinylacetate copolymer and organo-modified silica. ***Green Process Synth,*** p. 1-10, 2016.

TRONE, J. L. ***Thermoplastics foams.*** Ohio: Sherwood Publishers, Hinckley, 1996.

XU, Z.; JIANG, X.; LIU, T.; HU, G.; ZHAO, L.; ZHU, Z.; YUAN, W. Foaming of polypropylene with supercritical carbon dioxide. ***J Supercrit Fluids,*** 41, p. 299-310, 2007.

YOO, J. J.; BALAKRISHNAN, K.; HUANG, J.; MEUNIER, V.; SUMPTER, B. G; SRIVASTAVA, A.; CONWAY, M.; REDDY, A. L. M.; YU, J.; VAJTAI, R.; AJAYAN, P. M. Ultrathin planar graphene supercapacitors. ***Nano Lett,*** v. 11, n. 4, p. 1423-1427, 2011.

YU, H.; ZHANG, B.; BULIN, C.; LI, R.; Xing R. High-efficient synthesis of graphene oxide based on improved Hummers method. ***Sci Rep,*** v. 6, n. 36143 p. 1-7, 2016.

YUAN, N. Y.; MA, F. F.; LIU, Y. B.; DING, J. N. High conductive ethylene vinyl acetate composites filled with reduced graphene oxide and polyaniline. ***Composites Part A***: Applied Science and Manufacturing, v. 43, n. 12, p. 2183-2188, 2012.

ZIMMERMANN, M. V. G.; SILVA, M. P.; ZATTERA, A. J.; SANTANA, R. M.C. Effect of nanocellulose fibers and acetylated nanocellulose fibers on properties of poly(ethylene-co-vinyl acetate) foams. ***J Appl Polym Sci,*** 134, p. 44760-44771, 2017.

ZIMMERMANN, M. V. G.; TURELLA, T. C.; SANTANA, R. M. C.; ZATTERA, A. J. Comparative study between poly(ethylene-co-vinyl acetate) - EVA expanded composites filled with banana fiber and wood flour. ***Mater Res,*** 17, p. 1535-1544, 2014.

ZIMMERMANN, M. V. G.; TURELLA, T. C, SANTANA, R. M. C.; ZATTERA, A. J. The influence of wood flour particle size and content on the rheological, physical, mechanical and morphological properties of EVA/Wood Cellular Composites. ***Mater Des,*** 51, p. 660-666, 2014.

Received: 16 June 2023 - Accepted: 12 February 2024.